(13) Teramachi, S.; Hasegawa, A.; Yoshida, S. *Macromolecules* **1983**, *16*, 542.
(14) O'Driscoll, K. F.; Kale, L. T.; Garcia Rubio, L. H.; Reilly, P. M. *J. Polym. Sci., Polym. Chem. Ed.* **1984**, *22*, 2777.
(15) Inagaki, H.; Tanaka, T. In *Developments in Polymer Characterization*; Dawkins, J. V., Ed.; Applied Science: Barking, UK, 1982; Vol. 3, pp 1–32.
(16) Inagaki, H.; Matsuda, H.; Kamiyama, F. *Macromolecules* **1968**, *1*, 520.
(17) Kotaka, T.; White, J. L. *Macrmolecules* **1974**, *7*, 106.
(18) Ogawa, T.; Ishitobi, W. *J. Polym. Sci., Polym. Chem. Ed.* **1983**, *21*, 781.
(19) Teramachi, S.; Hasegawa, A.; Shima, Y.; Akatsuka, A.; Nakajima, M. *Macromolecules* **1972**, *12*, 992.
(20) Sato, H.; Takeuchi, H.; Suzuki, S.; Tanaka, Y. *Makromol. Chem., Rapid Commun.* **1984**, *5*, 719.
(21) Ogawa, T.; Sakai, M. *J. Polym. Sci., Polym. Phys. Ed.* **1981**, *19*, 1377.
(22) Teramachi, S.; Esaki, H. *Polym. J. (Tokyo)* **1975**, *7*, 593.
(23) Glöckner, G.; Koningsveld, R. *Makromol. Chem., Rapid Commun.* **1983**, *4*, 529.
(24) Danielewicz, M.; Kubín, M. *J. Appl. Polym. Sci.* **1981**, *26*, 951.
(25) Danielewicz, M.; Kubín, M.; Vozka, S. *J. Appl. Polym. Sci.* **1982**, *27*, 3629.
(26) Stejskal, J.; Kratochvíl, P. *Macromolecules* **1978**, *11*, 1097.
(27) Arranz, F.; Sánchez-Chaves, M.; Molinero, A.; Martínez, R. *Makromol. Chem., Rapid Commun.* **1983**, *4*, 297.
(28) Teramachi, S.; Kato, Y. *J. Macromol. Sci., Chem.* **1970**, *4*, 1785.
(29) Teramachi, S.; Kato, Y. *Macromolecules* **1971**, *4*, 54.
(30) Teramachi, S.; Fukao, T. *Polym. J. (Tokyo)* **1974**, *6*, 532.
(31) Bourguignon, J. J.; Bellissent, H.; Galin, J. C. *Polymer* **1977**, *18*, 937.
(32) Stejskal, J.; Kratochvíl, P.; Straková, D. *Macromolecules* **1981**, *14*, 150.
(33) Guyot, A.; Guillot, J. *J. Chim. Phys.* **1964**, *61*, 1434.
(34) Spinner, I. H.; Lu, B. C.-Y.; Graydon, W. F. *J. Am. Chem. Soc.* **1955**, *77*, 2198.
(35) Ring, W. *Makromol. Chem.* **1967**, *101*, 145.
(36) Myagchenkov, V. A.; Frenkel', S. Ya. *Vysokomol. Soedin., Ser. A* **1969**, *11*, 2348.
(37) Kruse, R. L. *J. Polym. Sci., Part B:* **1967**, *5*, 437.
(38) Stejskal, J.; Janča, J.; Kratochvíl, P. *Polym. J. (Tokyo)* **1976**, *6*, 549.
(39) Kratochvíl, P.; Straková, D.; Stejskal, J. *Polym. Commun.* **1985**, *26*, 202.
(40) Petrak, K. L.; Pitts, E. *Polymer* **1983**, *24*, 729.
(41) Stejskal, J.; Straková, D.; Procházka, O.; Kratochvíl, P. *Collect. Czech. Chem. Commun.* **1983**, *48*, 2656.
(42) Numerical values of data presented in figures are available on request.

Characterization of Poly(1,4-phenyleneterephthalamide) in Concentrated Sulfuric Acid. 4. Dilute and Semidilute Solution Regimes

Qicong Ying and Benjamin Chu*

Departments of Chemistry and Materials Science and Engineering, State University of New York at Stony Brook, Long Island, New York 11794-3400. *Received October 9, 1985*

ABSTRACT: From our analysis of the concentration and angular dependence of the static and dynamic properties (excess Rayleigh ratio ΔR_{vv}, radius of gyration R_g, hydrodynamic radius R_h, characteristic decay time Γ^{-1}, and second virial coefficients A_2 and k_d) of poly(1,4-phenyleneterephthalamide) (PPTA) in concentrated sulfuric acid (with and without the addition of a small amount of K_2SO_4), we have been able to examine the crossover behavior from the dilute to the semidilute solution regime for a rodlike polymer in solution. According to the scaling theory, the overlap concentration C^* for random coils is $\sim M/(N_A R_g^3)$, with M and N_A being the molecular weight and the Avogadro number, respectively. For rod macromolecules, $M/(N_A L^3) \lesssim C^*$. From semidilute to concentrated solution, an additional crossover behavior takes place. For rod macromolecules, $C^{**} \lesssim M/(N_A d L^2)$, with d and L being the rod diameter and length, respectively. In plots of $\lim_{K\to 0}[\Delta R_{vv}/(HC)]$ vs. concentration, the concentration C_m at which $\lim_{K\to 0}[\Delta R_{vv}/(HC)]$ shows a minimum can be represented by a modified Doi–Edwards inequality: $C_m \lesssim M/(N_A d^* L^{*2})$, with d^* and L^* being an effective diameter and an effective length of the macromolecule. K is the magnitude of the momentum transfer vector, ΔR is the excess Rayleigh ratio, and H is an optical constant. In a plot of $\log [M_{app}(HC/\Delta R_{vv}) - 1]$ vs. $\log (C/C_m)$, where M_{app} is the apparent molecular weight, the slope is equal to 1 for $C < C_m$ as de Gennes has predicted. The correlation length corresponding to the apparent root mean square radius of gyration at finite concentration was found to increase sharply above C_m, similar to the observation made by Burchard for aqueous poly(vinylpyrrolidone) solutions in the semidilute solution region.

I. Introduction

In previous papers,[1-3] we have characterized the dilute solution properties of poly(1,4-phenyleneterephthalamide) (PPTA) in concentrated sulfuric acid (with and without a small amount of K_2SO_4) using light scattering (LS) intensity and line-width measurements. We have been able to estimate the molecular weight dependences of intrinsic viscosity, of radius of gyration $\langle R_g \rangle_z^{1/2}$, and of translational diffusion coefficient D_z as well as the persistence length ρ ($\sim$290 Å) of PPTA in concentrated sulfuric acid. In addition, we have been able to estimate the molecular weight distributions of unfractionated PPTA samples[3] and to devise a simple calibration technique capable of monitoring molecular weight as well as molecular weight polydispersity index changes.[4] In this article, we present the crossover behavior for PPTA in concentrated sulfuric acid, with and without the addition of a small amount of K_2SO_4. Rodlike polymers are prone to interchain association.[5] Therefore, at higher solution concentrations interchain interactions may play an important role in the crossover behavior from the dilute to the semidilute solution regime. The behavior of the threshold concentration from dilute to semidilute solution is controlled by chain rigidity as well as molecular size. All experiments, including sample preparation and instrumentation, follow the same procedures as described in detail elsewhere.[2,3]

II. Dilute Solution Properties

Dynamic light scattering (LS) in combination with static light scattering intensity measurements has been shown to be a valuable approach to deduce information about macromolecular size, shape, molecular weight distribution,

0024-9297/86/2219-1580$01.50/0

and interactions. In static LS measurements, the excess Rayleigh ratio ΔR (ΔR_{vv} or ΔR_{hv}, vertical and horizontal components of excess Rayleigh ratio using vertically polarized incident light) and the weight-average molecular weight M_w are related according to the expressions

$$HC/\Delta R_{vv}(C,K=0) = 1/M_{app} + 2A_2C \quad (1)$$

$$HC/\Delta R_{vv}(C=0,K) = (1/M_{app})(1 + \langle R_g^2\rangle_{app}K^2/3 + ...) \quad (2)$$

$$M_{app} = M_w(1 + 4\delta^2/5) \quad (3)$$

$$\langle R_g^2\rangle_{app} = \langle R_g^2\rangle[(1 - 4\delta/5 + 4\delta^2/7)/(1 + 4\delta/5)] \quad (4)$$

where $H = [4\pi^2n^2/(N_A\lambda_0^4)](\partial n/\partial C)^2$ and $K = (4\pi n/\lambda_0)(\sin(\theta/2))$. The molecular anisotropy δ can be calculated from the ratio of ΔR_{vv} and ΔR_{hv} at zero scattering angle and infinite dilution by the relation $\Delta R_{vv}^0/\Delta R_{hv}^0 = 3\delta^2/(5 + 4\delta^2)$, where the superscript zero denotes extrapolation of the excess Rayleigh ratio to zero scattering angle at infinite dilution.

In the self-beating mode, the intensity time correlation function $G^{(2)}(t)$ is related to the first-order electric field time correlation function $g^{(1)}(t)$ by

$$G^{(2)}(t) = A(1 + b|g^{(1)}(t)|^2) \quad (5)$$

where A is the background and the coherence factor, b, is assumed to be an adjustable fitting parameter. In the cumulant expansion

$$\ln g^{(1)}(t) = -\bar{\Gamma}t + \sum(-1)^i\frac{\mu_i t^i}{i!} \quad (6)$$

At small scattering angles, the first cumulant $\bar{\Gamma}$ is related to the average translational diffusion coefficient $\bar{D}$ by

$$\lim_{K\to 0}\bar{\Gamma} = K^2\bar{D} \quad (7)$$

with

$$\bar{D} = \bar{D}_z^0(1 + k_dC) \quad (8)$$

At larger scattering angles, eq 7 is modified to yield

$$\bar{\Gamma}/K^2 \cong \bar{D}(1 + f\langle R_g^2(C)\rangle_{app}K^2) \quad (9)$$

which shows a similar concentration and angular dependence as those of eq 1 and 2. Thus, Burchard and Eisele[6] suggested a modified Zimm plot using $\bar{\Gamma}/K^2$ according to eq 8 and 9. In our case, the angular dependence of $\bar{\Gamma}/K^2$ vs. K^2 for solutions of PPTA in concentrated sulfuric acid without and with the addition of a small amount salt (K_2SO_4), as shown respectively in parts a and b of Figure 1, suggests a noticeable deviation from only the K^4-order expansion of eq 9. Thus, for PPTA solutions, we must be particularly careful in trying to obtain reliable extrapolation results. By using a semilogarithmic relationship, as sometimes practiced in light scattering intensity data analysis, the extrapolation procedure to zero scattering angle can be improved. Thus, eq 9 is rewritten as

$$\ln(\bar{\Gamma}(0,K)/K^2) \simeq \ln\bar{D}_z^0 + \ln[1 + f\langle R_g^2\rangle_{app}K^2] \quad (10)$$

with $\bar{\Gamma}(0,K)$ denoting $\bar{\Gamma}(C,K)$ at infinite dilution. In our case, the mean square radius of gyration $\langle R_g^2\rangle \sim 10^{-11}$ cm^2, $K^2 \sim 10^{10}$ cm^2, and $f < 1$, so $[f\langle R_g^2\rangle_{app}K^2]^2 < 1$. Since $\ln(1 + X) = X - (1/2)X^2 + (1/3)X^3 - ...$ for $X^2 < 1$, eq 10 becomes

$$\ln(\bar{\Gamma}(0,K)/K^2) \cong \ln\bar{D}_z^0 + f\langle R_g^2\rangle_{app}K^2 \quad (11)$$

Figure 2 shows a plot of $\ln(\bar{\Gamma}/K^2)$ vs. K^2 for sample 4 in 96% H_2SO_4 solutions. In Figure 2, all $\bar{\Gamma}$'s were evaluated by using the third-order cumulant fit. In comparison with those from the second-order cumulant fit, we found the

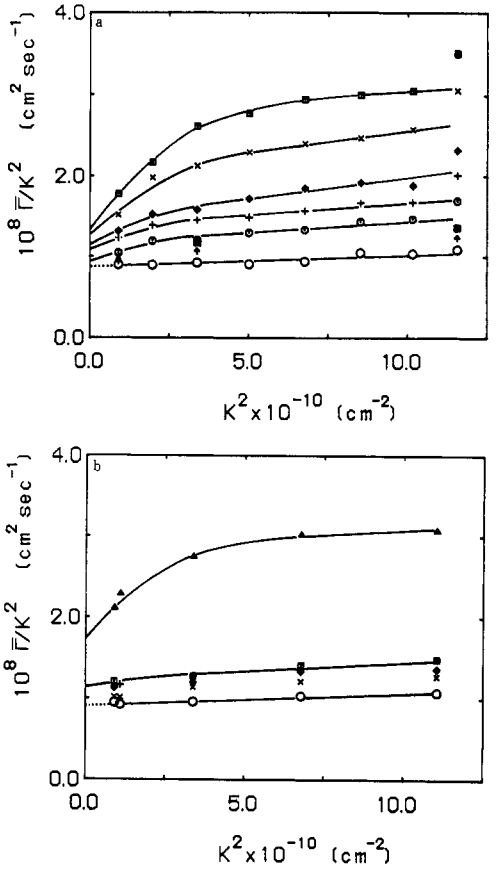

Figure 1. (a) Plots of $\bar{\Gamma}/K^2$ vs. K^2 for sample 4 (third-order cumulant fit) in 96 wt % H_2SO_4 at different concentrations: (○) $C = 0$, (↑) $C = 0.40 \times 10^{-3}$, (■), $C = 0.72 \times 10^{-3}$, (⊙) $C = 1.18 \times 10^{-3}$, (+) $C = 2.14 \times 10^{-3}$, (♦) $C = 2.80 \times 10^{-3}$, (×) $C = 4.54 \times 10^{-3}$, and (□) $C = 6.36 \times 10^{-3}$ g/mL. Solid curves are freely drawn to illustrate the noticeable deviation from the K^4-order expansion of $\bar{\Gamma}$ at finite concentrations and K values. (b) Plots of $\bar{\Gamma}/K^2$ vs. K^2 for sample 4 (third-order cumulant fit) in 96 wt % H_2SO_4 + 0.05 M K_2SO_4 at different concentrations: (○) $C = 0$, (×) $C = 0.60 \times 10^{-3}$, (♦) $C = 1.04 \times 10^{-3}$, (+) $C = 1.30 \times 10^{-3}$, (□) $C = 1.70 \times 10^{-3}$, and (▲) $= 7.68 \times 10^{-3}$ g/mL. Solid curves are freely drawn to illustrate the noticeable deviation from the K^4-order expansion of $\bar{\Gamma}$ at finite concentrations and K values.

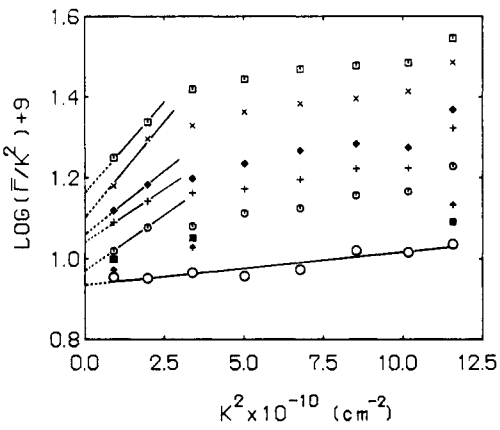

Figure 2. Plots of log $(\bar{\Gamma}/K^2) + 9$ vs. K^2 for sample 4 in 96% H_2SO_4 based on data in Figure 1a. Initial slopes are shown to illustrate the extrapolation procedure for $K \to 0$. Similar values of $\lim_{K\to0,C\to0}(\bar{\Gamma}/K^2)$ are obtained by using a second-order cumulant fit.

extrapolated $\bar{\Gamma}$ values to be in reasonable agreement, independent of the fitting procedure. The use of eq 10 and 11 instead of eq 9 is not necessary whenever $f\langle R_g^2\rangle_{app}K^2 < 1$. In our case, we obtained similar results by either means. Values of the variance $\mu_2/\bar{\Gamma}^2$ tend to increase with

Table I
Static and Dynamic Properties of PPTA in Concentrated Sulfuric Acid with and without Added Salt

sample	solvent	$M_w \times 10^{-4}$	$\bar{D}_z \times 10^8$,[a] cm²/s	R_h,[b] nm	R_g,[c] nm	f
5	96 wt % H_2SO_4	4.83	0.72	18.2	48	0.06
4	96 wt % H_2SO_4	3.84	0.88	14.9	33	0.21
3	96 wt % H_2SO_4	2.27	1.13	11.5	22	0.29
2	96 wt % H_2SO_4	1.59	1.59	8.2		
1	96 wt % H_2SO_4	1.45	1.96	6.7		
5	96 wt % H_2SO_4 + 0.05 M K_2SO_4	4.26	0.74	17.6	35	0.30
4	96 wt % H_2SO_4 + 0.05 M K_2SO_4	2.98	0.93	14.1	34	0.19
3	96 wt % H_2SO_4 + 0.05 M K_2SO_4		0.99	13.1		
2	96 wt % H_2SO_4 + 0.05 M K_2SO_4		1.57	8.3		

[a] $\bar{D}_z$ is the z-average diffusion coefficient with an estimated precision of a few percent. [b] R_h is the average hydrodynamic radius, with $\bar{D}_z = k_BT/(6\pi\eta_0 R_h)$. [c] $R_g \equiv \langle R_g^2\rangle_z^{1/2}$; $\langle R_g^2\rangle_{app}$ can be computed according to eq 4 using δ values listed in ref 2.

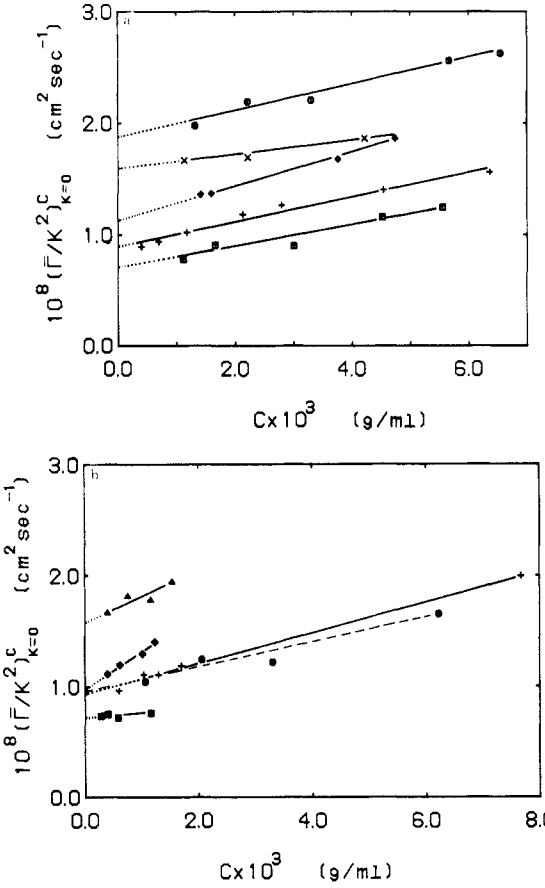

Figure 3. (a) Plots of $\lim_{K\to 0}(\bar{\Gamma}/K^2)$ (third-order cumulant fit) vs. concentration for PPTA samples in 96% H_2SO_4: (■) sample 5; (+) sample 4; (♦) sample 3; (×) sample 2; (○) sample 1. (b) Plots of $\lim_{K\to 0}(\bar{\Gamma}/K^2)$ (third-order cumulant fit) vs. concentration for PPTA samples in 96% H_2SO_4 + 0.05 M K_2SO_4: (■) sample 5; (+) sample 4; (♦) sample 3; (▲) sample 2; (●) sample 4 in 96% H_2SO_4 + 0.005 M K_2SO_4.

increasing concentration and increasing scattering angle. In Figure 2 $\bar{\Gamma}/K^2$ seems to deviate from the K^2 dependence at K^2 equal to $\sim 4 \times 10^{10}$ cm^{-2}. Thus, values of $\bar{\Gamma}(C,K=0)/K^2$ were evaluated from the intercepts by using the initial slope at relatively low scattering angles $K^2 < 4 \times 10^{10}$ cm^{-2}. Parts a and b of Figure 3 show plots of $\bar{\Gamma}(C,0)/K^2$ vs. concentration for five PPTA samples in 96% H_2SO_4 and 96% H_2SO_4 + 0.05 M K_2SO_4, respectively. From a linear concentration dependence of $\bar{\Gamma}(C,0)/K^2$, we have

$$\bar{\Gamma}(C,0)/K^2 = \bar{D}_z^0 + k_d^* C \tag{12}$$

with $k_d^* = \bar{D}_z^0 k_d$. $k_d \sim 125$ cm^3/g for samples 3, 4, and 5 in 96% H_2SO_4, which is higher than those we estimated

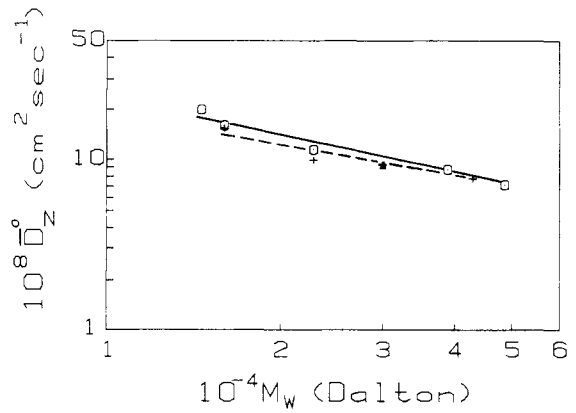

Figure 4. log–log plots of $\bar{D}_z^0$ vs. M_w at 30 °C, where $\bar{D}_z^0$ and M_w denote the z-average translational diffusion coefficient at infinite dilution and the weight-average molecular weight, respectively. Hollow rectangles, in H_2SO_4; solid line denotes $\bar{D}_z^0 = 2.72 \times 10^{-5} M_w^{-0.77}$ cm²/s; triangle, in H_2SO_4 + 0.005 M K_2SO_4; crosses, in H_2SO_4 + 0.05 M K_2SO_4; dashed line denotes $\bar{D}_z^0 = 1.51 \times 10^{-5} M_w^{-0.72}$ cm²/s. Note the suggested slight difference for PPTA in H_2SO_4 with and without added salt.

in paper 1.[2] Nevertheless, k_d does not show a strong molecular weight dependence within the molecular weight range of our studies ($(2.3–4.8) \times 10^4$). For the other two lower molecular weight samples, k_d was estimated to be 45 cm³/g. In fact, more experimental work should be done in order to evaluate the relatively weak molecular weight dependence of k_d. Values of $\bar{D}_z^0$ and the corresponding hydrodynamic radius R_h are listed in Table I. We used

$$R_h = k_BT/(6\pi\eta_0\bar{D}_z^0) \tag{13}$$

where k_B and η_0 are the Boltzmann constant and the solvent viscosity, respectively. The molecular weight dependence of $\bar{D}_z^0$ for PPTA in 96% H_2SO_4 (with and without added K_2SO_4) is shown in Figure 4. For PPTA in 96% H_2SO_4 at 30 °C, least-squares fitting results show

$$\bar{D}_z^0 = 2.72 \times 10^{-5} M_w^{-0.77} \text{ cm}^2/\text{s} \tag{14}$$

$$R_h = 4.78 \times 10^{-10} M_w^{0.77} \text{ cm} \tag{15}$$

and in 96% H_2SO_4 + 0.05 M K_2SO_4

$$\bar{D}_z^0 = 1.51 \times 10^{-5} M_w^{-0.72} \text{ cm}^2/\text{s} \tag{16}$$

$$R_h = 8.63 \times 10^{-10} M_w^{0.72} \text{ cm} \tag{17}$$

In Figure 4 the slopes in 96% H_2SO_4 and in 96% H_2SO_4 + 0.05 M K_2SO_4 appear to agree within experimental error limits; i.e., the values (0.77 and 0.72) are not far from $\sim$0.75, which we estimated in paper 1[2] without careful extrapolation of $\bar{\Gamma}/K^2$ to zero scattering angle. The molecular weight dependence for the radius of gyration is shown in Figure 5. Our data suggest that $\langle R_g^2\rangle_z^{1/2} = 9.21$

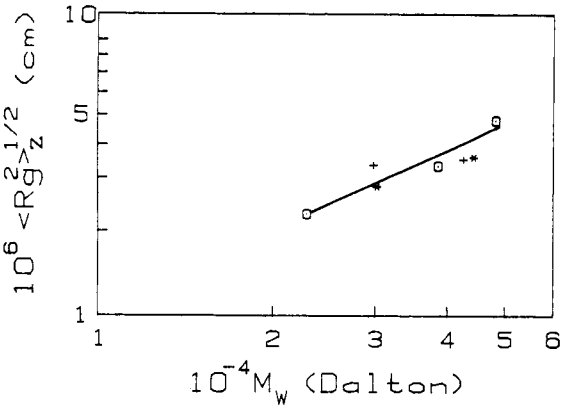

Figure 5. log–log plot of $\langle R_g^2 \rangle^{1/2}$ vs. M_w for PPTA in 96% H_2SO_4 (○), in 96% H_2SO_4 + 0.005 M K_2SO_4 (*), and in 96% H_2SO_4 + 0.05 M K_2SO_4 (+). Solid line denotes $\langle R_g^2 \rangle^{1/2} = 9.21 \times 10^{-10} M_w^{0.78}$ cm.

$\times 10^{-10} M_w^{0.78}$, with R_g expressed in cm. An α_{R_g} exponent of 0.78 for PPTA in 96% H_2SO_4 also seems to have a higher value than that for PPTA in H_2SO_4 with K_2SO_4. Perhaps the PPTA chain appears to be more rigid in H_2SO_4 than the same chain in H_2SO_4 with added salt, or perhaps some side-by-side salt association could increase the overall rigidity of the system.

Wilcoxon and Schurr[7] presented an equation that deals with the angular dependence of $D_{app}(K) = (\bar{\Gamma}/K^2)$ for rigid rods

$$D_{app}(K) = \bar{D}_z^0 + 2\Delta(1/3 - F(KL)) + 2L^2 D_R G(KL) \quad (18)$$

where $F(KL)$ and $G(KL)$ are universal functions of KL and are independent of molecular weight. It should be noted that eq 9 describes the general K^2 expansion of $\bar{\Gamma}/K^2$ for macromolecular solutions, irrespective of polymer shape, and is valid for random coils and semiflexible chains, as well as rigid rods, while eq 18 is valid only for rigid rods. Wilcoxon and Schurr calculated values of $F(KL)$ and $G(KL)$ from $KL = 0$ to infinity and listed the results in their Table 1 of ref 7. Thus, $D_{app}(K)$ can be calculated by using eq 18 for any thin rods for which $\bar{D}_z^0$, Δ, L, and D_R are known. Δ ($=D_\parallel - D_\perp$) is the anisotropy of the translational diffusion coefficient, with $D_\perp$ and $D_\parallel$ being the translational diffusion coefficients perpendicular and parallel to the rod axis, respectively. Using Broersma's relations,[8] one can express the rotational diffusion coefficient D_R and other quantities:

$$D_\parallel = (k_B T/2\pi\eta_0 L)(s - r_\parallel) \quad (19)$$

$$D_\perp = (k_B T/4\pi\eta_0 L)(s - r_\perp) \quad (20)$$

$$D_R = (3k_B T/(\pi\eta_0 L^3))(s - \zeta) \quad (21)$$

where

$$s = \ln(2L/d) \quad (22)$$

$$r_\parallel = 1.27 - 7.4((1/s) - 0.34)^2 \quad (23)$$

$$r_\perp = 0.19 - 4.2((1/s) - 0.39)^2 \quad (24)$$

$$\zeta = 1.45 - 7.5(1/s - 0.27)^2 \quad (25)$$

The angular dependence of $D_{app}(C=0,K)$ can be calculated from eq 18 and is represented in parts a and b of Figure 6 by the dashed line for five PPTA samples in 96% H_2SO_4 and 96% H_2SO_4 + 0.05 M K_2SO_4, respectively. The agreement between the experimentally measured points and the dashed curve appears to be fair for high molecular weight samples; but the disparity is obvious for the lower molecular weight samples. $\bar{D}_z^0(C=0,K=0) = 0.88 \times 10^{-8}$ cm^2/s for sample 4 in Figure 6a, as listed in Table I, while

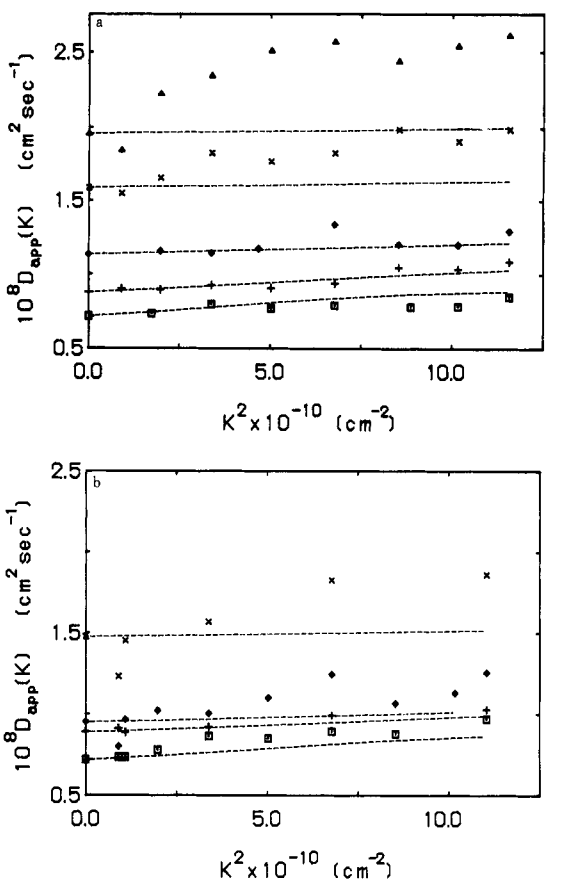

Figure 6. (a) Plots of $D_{app}(K) = (\bar{\Gamma}(0,K)/K^2)$ vs. K^2 for PPTA in 96% H_2SO_4. Dashed lines are calculated from Schurr's equation, eq 18. (□) sample 5; (+) sample 4; (♦) sample 3; (×) sample 2; (▲) sample 1. (b) Plots of $D_{app}(K) = (\bar{\Gamma}(0,K)/K^2)$ vs. K^2 for PPTA in 96% H_2SO_4 + 0.05 M K_2SO_4. Dashed lines are calculated from Schurr's equation 18. (□) sample 5; (+) sample 4; (♦) sample 3; (×) sample 2.

Table II
Average Persistence Length per Chain (L_w/ρ) of PPTA in 96% H_2SO_4 with and without Added Salt[a]

sample	solvent	$M_w \times 10^{-4}$	L_w, nm	L_w/ρ
5	96 wt % H_2SO_4	4.83	256	9
4	96 wt % H_2SO_4	3.84	203	7
3	96 wt % H_2SO_4	2.27	120	4
2	96 wt % H_2SO_4	1.59	84	3
1	96 wt % H_2SO_4	1.45	77	3
5	96 wt % H_2SO_4 + 0.005 M K_2SO_4	4.42	234	12
4	96 wt % H_2SO_4 + 0.005 M K_2SO_4	3.03	160	8
5	96 wt % H_2SO_4 + 0.05 M K_2SO_4	4.26	226	11
4	96 wt % H_2SO_4 + 0.05 M K_2SO_4	2.98	158	8

[a] $L_w = (M_w/M_o) \times l_o = (M_w/238) \times 1.26$ nm; ρ = 29-nm persistence length of PPTA in 96% H_2SO_4; ρ = 20-nm persistence length of PPTA in 96% H_2SO_4 + (0.05 or 0.005 M) K_2SO_4.

$\bar{D}_z^0$ [$\equiv \lim_{C\to 0,K\to 0} \bar{\Gamma}/K^2$] = 0.86×10^{-8} cm^2/s according to Figure 1a.

The Wilcoxon–Schurr eq 18 for rigid rods cannot be expected to hold for semiflexible chains. Table II lists the average number of persistence lengths per chain (L_w/ρ) of the PPTA samples we have investigated. The angular dependence of $D_{app}(C=0,K)$ can be represented by eq 11 in a semilogarithmic plot where we have been able to evaluate f, a dimensionless parameter defined by Stockmayer and Schmidt,[9] from the slopes and values of $\langle R_g^2 \rangle_{app}$ according to eq 11, as listed in Table I. For unfractionated

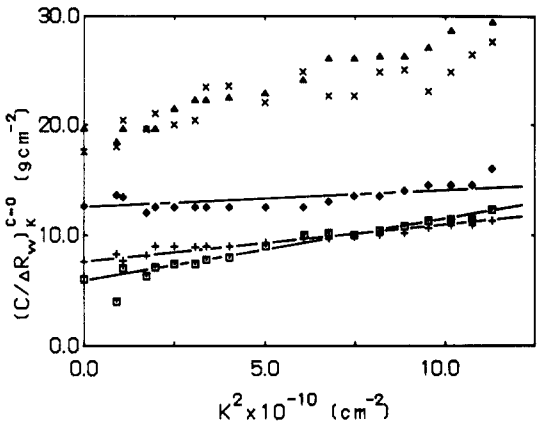

Figure 7. Plots of $(C/\Delta R_{vv})_K^{C=0}$ vs. K^2 for PPTA (samples 1–5) in 96% H_2SO_4: (□) sample 5; (+) sample 4; (▲) sample 3; (×) sample 2; (♦) sample 1. R_g values for samples 3–5 are listed in Table I.

PPTA samples with weight-average molecular weights varying from 2×10^4 to 5×10^4, $f \sim 0.2$–0.3 for $L_w/2\rho$ ranging from 2 to 4.4, where $L_w = N_w l_0$ with repeating unit length $l_0 = 12.6$ Å and $N_w = M_w/238$ for PPTA assuming that $\rho = 290$ Å.

The concentration and angular dependence of $D_{app}(C,K)$ can be expressed finally by

$$\ln (\bar{\Gamma}(C,K)/K^2) = \ln (\bar{\Gamma}(0,0)/K^2) + \ln (1 + k_d C) + F^* K^2 \quad (26)$$

where $F^* = f\langle R_g^2(C)\rangle_{app}$ ($\equiv f\xi^2$, with ξ being the correlation length) and we have taken $\ln (1 + F^*K^2) \simeq F^*K^2$. As C approaches zero

$$\ln (\bar{\Gamma}(0,K)/K^2) = \ln (\bar{\Gamma}(0,0)/K^2) + F_0^* K^2 \quad (27)$$

where we have taken F_0^* to be the value of F^* at infinite dilution. The change of F^* with respect to concentration comes mainly from the effective size change with respect to concentration. As K approaches zero

$$(\bar{\Gamma}(C,0)/K^2) = (\bar{\Gamma}(0,0)/K^2) + k_d^*(K=0)C \quad (28)$$

Thus, the term $(\bar{\Gamma}(0,0)/K^2)$ can be evaluated from plots of $(\bar{\Gamma}(C,K)/K^2)$ vs. concentration and scattering angle according to eq 27 and 28, similar to the Zimm plot used in static LS data analysis, as shown in Figure 7.

III. Overlap Threshold between Dilute and Semidilute Solution Regimes

According to the scaling theory for athermal polymer solutions, the osmotic pressure is related to C/C^* at constant temperature T as

$$(\Pi/T) = (C/N)f(C/C^*) \quad (29)$$

where C is the concentration; N, the degree of polymerization; and C^*, the overlap threshold concentration from dilute to semidilute solutions. In dilute solution $f(C/C^*)$ is expressed as

$$f(C/C^*) = 1 + B(C/C^*) + \ldots \quad (30)$$

where B is a constant. According to eq 29 and 30, we have

$$\Pi/T = (C/N)[1 + B(C/C^*) + \ldots] \quad (31)$$

Then the osmotic compressibility $(\Delta\Pi/\Delta C)_{T,P}$ at constant temperature T and pressure P has the form

$$(N/T)(\partial\Pi/\partial C)_{T,P} = 1 + 2B(C/C^*)$$

or

$$\log [(N/T)(\partial\Pi/\partial C) - 1] = \log (\text{constant}) + \log (C/C^*) \quad (32)$$

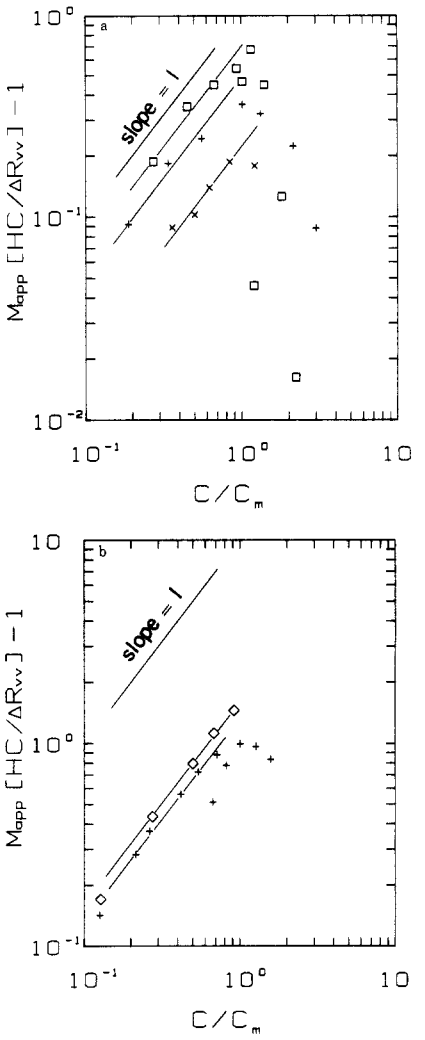

Figure 8. (a) Plots of log $[M_{app}(HC/\Delta R_{vv}) - 1]$ vs. log (C/C_m) for PPTA in 96% H_2SO_4: (□) sample 5; (+) sample 4; (×) sample 2. (b) Plots of log $[M_{app}(HC/\Delta R_{vv}) - 1]$ vs. log (C/C_m) for PPTA (sample 4) in 96% H_2SO_4 + 0.05 M K_2SO_4 (◇) and 96% H_2SO_4 + 0.005 M K_2SO_4 (+).

where we have dropped the subscripts T and P for the osmotic compressibility. In a plot of log $[(N/T)(\partial\Pi/\partial C) - 1]$ vs. log (C/C^*) the slope is equal to 1 in the dilute solution regime.

In a previous paper[2] we report a minimum value for $\Delta R_{vv}/(HC)$ occurring at concentration C_m in a plot of $\Delta R_{vv}/(HC)$ vs. concentration at constant molecular weight. Parts a and b of Figure 8 show plots of log $[M_{app}(HC/\Delta R_{vv}) - 1]$ vs. log (C/C_m) for PPTA in 96% H_2SO_4 and 96% H_2SO_4 + 0.05 M (or 0.005 M) K_2SO_4, where M_{app} is the apparent molecular weight. In the concentration region $C < C_m$, the slopes for all three PPTA samples are close to one, indicating dilute solution behavior. Small deviations in slope ($\approx$1) appear to occur for $C \lesssim C_m$. For $C > C_m$, log $[(M_{app})(HC/\Delta R_{vv}) - 1]$ drops down sharply with increasing concentration, and the decrease does not appear to correlate with molecular weight. The results suggest that for wormlike chains, the dilute solution behavior covers a concentration range much greater than $M/(N_A L^3)$.

The correlation length ξ $[=\langle R_g^2(C)\rangle_{app}^{1/2}]$ equivalent to the apparent root mean square radius of gyration at finite concentration C is influenced by interactions among chains. In a double-logarithmic plot, parts a and b of Figure 9 show ξ^2 as a function of C/C_m for PPTA in H_2SO_4 and H_2SO_4 + 0.05 M K_2SO_4, respectively. ξ^2 increases with increasing C/C_m up to $C = C_m$; beyond C_m the slope appears to in-

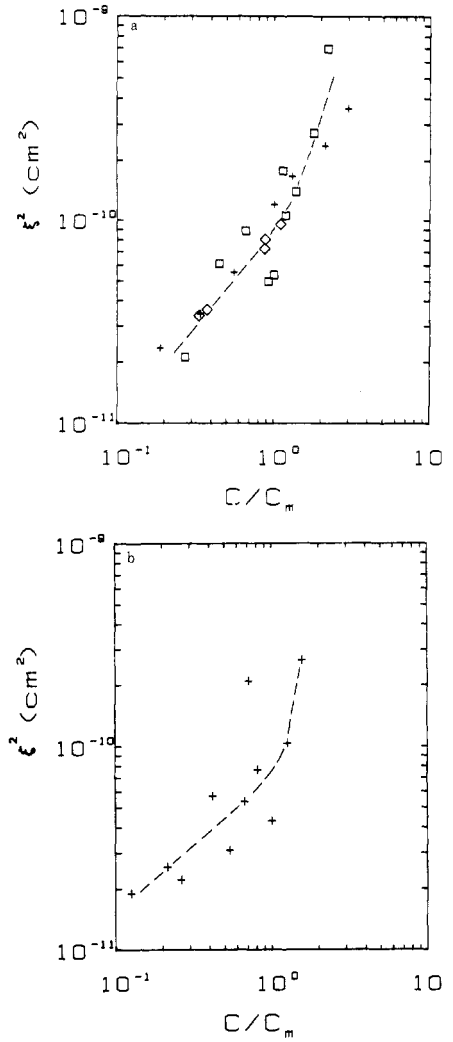

Figure 9. (a) log–log plots of ξ^2 vs. C/C_m for PPTA sample 5, (□), sample 4 (+), and sample 3 (◇) in 96% H_2SO_4. The dashed curve is used to suggest the appearance of an increasing slope for $C > C_m$. (b) log–log plots of ξ^2 vs. C/C_m for PPTA sample 4 in 96% H_2SO_4 + 0.005 M K_2SO_4. The dashed curve is used to suggest the appearance of an increasing slope for $C > C_m$.

crease even more sharply for PPTA in 96% H_2SO_4 with and without added salt, similar to the observations made by Burchard for aqueous poly(vinylpyrrolidone) solutions in semidilute solutions.[6] Interchain association could be one possible reason for this additional increase as well as the curvature noted at high concentrations in Figure 1. However, we have no experimental evidence to prove the actual causes for the additional changes. Doi and Edwards[10] have shown that the overlap concentration for rigid rods $C^{**} < M/(N_A d L^2)$. With $M_w = M_0 N_w$ and $L = l_0 N_w$, the inequality can be rewritten as

$$C^{**} < M_0/(N_A d l_0 L) \text{ (g/cm}^3\text{)} \quad (33)$$

where M_0 and l_0 are the weight and the length of each repeating unit. According to the inequality (33), C^{**} is proportional to the reciprocal of contour length L.

From our experimental results, we clearly see the dilute solution behavior at $C < C_m$. Beyond C_m, the solution behavior is correlated to the macromolecular size and changes sharply with increasing concentration. Thus, it is perhaps more reasonable to regard C_m as the overlap threshold concentration from the semidilute to the concentrated solution regime. Values of C_m (expressed in g/cm^3) for four PPTA samples with different molecular weights are listed in Table III. Within our experimental error limits, C_m appears to be relatively independent of molecular weight. Consequently, we view the crossover behavior for wormlike chains (PPTA in concentrated sulfuric acid) with a modified perspective. Rodlike polymers are prone to interchain association.[4] The effect of association is expected to occur in semidilute solutions where macromolecules are more likely to have contact with one another. On the other hand, the probability for macromolecules to be associated with one another is proportional to the macromolecular chain rigidity. The shorter chains are more rigid and are easier to be associated with one another. Therefore, if we take C_m as the concentration at which macromolecules touch one another, the magnitude of C_m can be expected to be influenced by both macromolecular size and chain rigidity. We define[12] an effective length L^*, which is related to the contour length L, and an effective diameter d^*.

Table III
Crossover Concentration of Rodlike Polymers in Solution

sample	solvent	$C_m \times 10^{-3}$, g/cm^3 obsd	$C_m \times 10^{-3}$, g/cm^3 computed[a]	$C^{**} \times 10^{-3}$,[b] g/cm^3
5	96 wt % H_2SO_4	2.5	2.5	2.0
4	96 wt % H_2SO_4	2.1	2.7	2.6
2	96 wt % H_2SO_4	1.8	3.4	6.2
1	96 wt % H_2SO_4	2.4	3.4	6.8
4	96 wt % H_2SO_4 + 0.005 M K_2SO_4	~4	~3.8	
4	96 wt % H_2SO_4 + 0.05 M K_2SO_4	~4.5	~3.8	

[a] $C_m = B^*\{M_w/[N_A(L/\rho)^{1/4}d\rho L]\}$ g/cm^3, where $B^* \sim 0.24$, ρ = 29-nm persistence length of PPTA in 96% H_2SO_4, and $\rho \sim$ 20-nm persistence length of PPTA in 96% H_2SO_4 + (0.05 or 0.005 M) K_2SO_4. [b] $C^{**} = M_0/(N_A d l_0 L)$ g/cm^3.

$$L^* = (\rho L)^{1/2} \quad (34)$$

$$d^* = (L/\rho)^{1/4} d \quad (35)$$

where we have assumed the molecular volume of a semiflexible chain to be independent of chain flexibility. Then for C_m, a similar inequality can be written as

$$C_m < M/(N_A d^* L^{*2}) \quad (36)$$

or

$$C_m \sim B^* M/(N_A d^* L^{*2}) \quad (37)$$

For rigid rods, the persistence length is L; we then retrieve eq 36 or

$$C_m < M_0/(N_A d l_0 L) \quad (38)$$

which is the same as the Doi–Edwards inequality for C^{**}.

For wormlike chains, ρ is shorter than the contour length L and thus $L^* < L$. In Table II, our data show that C_m for PPTA in concentrated sulfuric acid with added salt appears to have a higher value than the one without added salt, corresponding to the fact that PPTA in concentrated sulfuric acid has a higher persistence length than those with added salt.[11] The experimental data for C_m and the results calculated from eq 38 with an adjustable parameter $B^* \sim 0.24$ and a persistence length ρ = 290 and 200 Å for PPTA in 96% H_2SO_4 and in H_2SO_4 + 0.005 M K_2SO_4, respectively, are in fairly good agreement. The introduction of effective L^* and d^* to take into account chain flexibility seems to retain, at least qualitatively, the crossover behavior from dilute to semidilute and from semidilute to concentrated solutions for wormlike chains.

In summary, we have found that by using a semilogarithmic relationship, log $\bar{\Gamma}(K)/K^2$ vs. K^2, $\bar{\Gamma}$ can be ex-

trapolated to zero scattering angle with more confidence. The translational diffusion coefficient at infinite dilution can be evaluated by using a modified Zimm plot (eq 27 and 28). We observed dilute solution behavior at $C < C_m$, at which concentration $[\Delta R_{vv}/(HC)]$ also shows a minimum. The concentration C_m $[\sim M/(N_A d^* L^{*2})]$ differs from C^{**} $[\sim M/(N_A d L^2)]$ for rigid rods. The solution behavior for semiflexible chains is correlated to the macromolecular size and changes sharply with increasing concentration (Figure 9). Thus, we consider it more reasonable to regard C_m as the threshold concentration from the semidilute to the concentrated solution regime. Furthermore, for wormlike chains, the concentration range between semidilute and concentrated solution regimes is more compressed.

Acknowledgment. We gratefully acknowledge the National Science Foundation, Polymers Program (Grant DMR 8314193) and the Petroleum Research Fund, administered by the American Chemical Society, for support of this research.

Registry No. PPTA (SRU), 24938-64-5; PPTA (copolymer), 25035-37-4; K_2SO_4, 7778-80-5.

References and Notes

(1) Chu, B.; Ying, Q.; Wu, C.; Ford, J. R.; Dhadwal, H.; Qian, R.; Bao, J.; Zhang, J.; Xu, C. *Polym. Commun.* **1984**, *25*, 211.
(2) Ying, Q.; Chu, B.; Qian, R.; Bao, J.; Zhang, J.; Xu, C. *Polymer* **1985**, *26*, 1401.
(3) Chu, B.; Ying, Q.; Wu, C.; Ford, J. R.; Dhadwal, H. S. *Polymer* **1985**, *26*, 1408.
(4) Chu, B.; Wu, C.; Ford, J. R. *J. Colloid Interface Sci.* **1985**, *105*, 473.
(5) Wong, C. P.; Ohnuma, H.; Berry, G. C. *J. Polym. Sci., Polym. Symp.* **1978**, *No. 65*, 173.
(6) Burchard, W.; Eisele, M. *Pure Appl. Chem.* **1984**, *56*, 1379.
(7) Wilcoxon, J.; Schurr, J. M. *Biopolymers* **1983**, *22*, 849.
(8) Broersma, S. J. *J. Chem. Phys.* **1960**, *32*, 1626, 1632.
(9) Stockmayer, W. H.; Schmidt, M. *Pure Appl. Chem.* **1982**, *54*, 407.
(10) Doi, M.; Edwards, S. F. *J. Chem. Soc., Faraday Trans. 2* **1978**, *74*, 560.
(11) Ying, Q.; Chu, B. *Makromol. Chem., Rapid Commun.* **1984**, *5*, 785.
(12) The details will be described separately by: Ying, Q.; Chu, B., to be published.

Application of Raman and Laser Light Scattering to the Melt Polymerization of Hexachlorocyclotriphosphazene. 1

Day-chyuan Lee,† James R. Ford, George Fytas,‡ and Benjamin Chu*

Department of Chemistry, State University of New York at Stony Brook, Long Island, New York 11794-3400

Gary L. Hagnauer

Polymer Research Division, Army Materials Technology Laboratory, Watertown, Massachusetts 02172-0001. *Received November 4, 1985*

ABSTRACT: The application of a novel laser light scattering apparatus is described for on-line monitoring of the high-temperature, melt polymerization of hexachlorocyclotriphosphazene (HCTP) and the in situ characterization of the poly(dichlorophosphazene) (PDP) product. A combination of Raman spectroscopy, angular measurement of absolute light scattering intensities, and Rayleigh line width (dynamic) light scattering measurements are employed. More conventional techniques are inappropriate due to the polymer's hydrolytic instability, the high temperature required for polymerization, and the nature and apparent complexity of the reaction. Concentrations of the reaction components and characteristics of the polymer, such as weight-average molecular weight (M_w) and z-average radius of gyration (R_g) in the dilute solution regime and the cooperative diffusion coefficient (D_c) and osmotic compressibility $[(\partial\Pi/\partial C)_{T,P}]$ in semidilute solutions, are monitored with polymerization time. Experimental results are found to be in excellent agreement with those obtained indirectly by the batchwise polymerization of the same material.

Introduction

Poly(organophosphazenes) comprise a promising new class of technological polymers usually prepared by the organosubstitution of chlorine atoms on poly(dichlorophosphazene) (I).[1-3] The precursor polymer I, a high molecular weight elastomer (T_g, −63 °C), reacts with moisture and therefore must be modified in order to obtain long-term hydrolytic stability and other useful properties. Depending upon the size and nature of the side group substituents, polymers with a wide range of physical properties may be produced.

The polymer I is prepared by the high-temperature (ca. 250 °C) ring-opening polymerization of hexachlorocyclotriphosphazene (II).[4] Polymerizations may be conducted in solution or in the cyclic trimer melt, and catalysts may

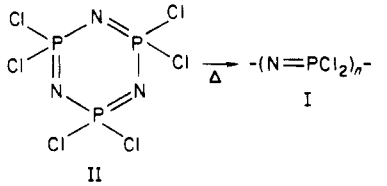

II I

be employed to reduce the reaction temperature and control polymer structure.[4,5] It is essential that II is highly pure and polymerization conditions are carefully controlled. If impurities are present or if the polymerization is allowed to continue too long or at too high a temperature, I may cross-link and thereby be unsuitable for organosubstitution.

The cyclic trimer II is a white crystalline (mp 112–114 °C) solid that sublimes under vacuum and is soluble in most organic solvents. The open-chain polymer I is soluble in a variety of solvents (e.g., benzene, trichlorobenzene, chloroform, and tetrahydrofuran) and typically has a high molecular weight ($M_w = 2 \times 10^6$) and broad molecular weight distribution ($M_w/M_n = 3$–7). Precautions must be

* Author to whom all correspondence should be addressed.
† Present address: Chemical Engineering Department, University of Wisconsin, Madison, Wisconsin 57305.
‡ Present address: Chemistry Department, University of Crete, PO Box 1470, 711 10 Iraklion Crete, Greece.

0024-9297/86/2219-1586$01.50/0